Shah, Z.; Rooman, M.; Asif Jan, M.; Vrinceanu, N.; Deebani, W.; Shutaywi, M.; Ferrándiz Bou, S. (2022). Radiative Darcy-Forchheimer Micropler Bödewadt flow of CNTs with viscous dissipation effect. Journal of Petroleum Science and Engineering. 217:1-11. https://doi.org/10.1016/j.petrol.2022.110857

Radiative Darcy-Forchheimer Micropler Bödewadt flow of CNTs with viscous dissipation effect

Zahir Shah[1], Muhammad Rooman[1], Muhammad Asif Jan[2], Narcisa Vrinceanu [3,*], Wejdan Deebani[4], Meshal Shutaywi[4], Santiago Ferrandiz Bou[5]

[1]*Department of Mathematical Sciences, University of Lakki Marwat, Lakki Marwat 28420, Khyber Pakhtunkhwa Pakistan*
[2]*Department of mathematics, Kohat University of Science and Technology KUST, Kohat 26000, Khyber pakhtoonkhwa, Pakistan*

[3] *Faculty of Engineering, Department of Industrial Machines and Equipments, "Lucian Blaga" University of Sibiu, 10 Victoriei Boulevard, 5500204, Romania*
[4]*Department of Mathematics College of Science & Arts, Rabigh King Abdul-Aziz University 21911, Saudi Arabia*

[5]*Dept. of Mechanical and Materials Engineering, Higher Polytechnic School of Alcoy Universitat Politècnica de València*

Corresponding authors: Zahir@ulm.edu.pk & vrinceanu.narcisai@ulbsibiu.ro

Abstract

This article goal to examine the three-dimensional micropolar nanofluids of single and multi-walled carbon nanotubes (CNTs) dissolved in water and gasoline liquids for the first time reported to the case of so-called classical Bödewadt flow, which occurs when a fluid rotates at an adequate great distance out of a static disk. The static disk is then stretched linearly in the radial direction. The Darcy-Forchheimer porous media is also taken into account. Energy equation is investigated in existence of convection and radiation. The effect of viscous dissipation is also taken into account. The flow field equations are converted from PDEs to ODEs using appropriate transformation. The implementation of the bvp4c technique (Shooting scheme) is use to construct solutions to these ODEs. In addition to Nusselt number, skin friction, axial velocity, radial velocity, tangential velocity, micro-rotational velocities and fluid temperature are all

investigated using physical factors. The finding indicates that the volume fraction enhanced, the micro-rotational velocities enhances. The tabulation outcomes indicates that the skin friction declined for escalating values of porosity parameter and volume fraction, while Nusselt number show opposite behavior. It was also discovered that the effect of multiple-walled CNTs is quite effective than that of single-walled CNTs. When compared to water-based fluids, gasoline oil also displays an overarching trend.

Keywords: Micropolar nanofluid; Darecy-Forchheimer; porous medium; heat transfer; viscous dissipation.

1. Introduction

The fluid thermal conductivity is critical for cumulative the heat transfer rate. Water, gasoline oil, and ethylene glycol fall within the classification of bad heat exchanger fluids due to their weak heat conductivity. The rate of heat transmission in these traditional liquids can be regulated by increasing thermal conductance. Furthermore, solid particles have large thermal conductivity than liquid particles. By incorporating such solid nanoscale size particles into the aforementioned traditional liquids, the thermal efficiency of such fluids can be increased. The base liquid is the fluid into which these nano-sized particles will be introduced, and the combination is known as nanomaterial or nanofluid. Metals, aluminum, silver, oxides, carbon, and carbides among other materials are used to make nanoparticles. Choi and Eastman [1] were the pioneer to utilize nanomaterials to enhance the base-liquid thermal conductivity. The heat transmission rate of nanomaterials is shown to be significantly reliant on the geometry of nano-sized particles. In separate study, Elias et al. [2] investigated the consequences of nanoparticles form on heat conduction and the outcomes of a shell-and-tube heat transfer. The analysis revealed that

cylindrical shape nanoparticles have good heat transfer capabilities and heat exchanger rate than other cylindrical shape nanoparticle shapes, whereas entropy formation for nanofluid with cylindrical shape nanoparticles was larger than for other nanoparticle shapes. Elias et al. [3] examined the influence of numerous nanoparticles forms on the total heat transfer rate, heat transfer coefficient, and entropy production of the shell-and-tube heat transfer with varying baffle angles. They reported that among the nanoparticle forms studied, cylindrical nanofluids had a greater thermal efficiency, and the entropy reduction rate is significantly greater for cylindrical shapes than for any additional forms at a 20^{o} baffle angle. Sheikholeslami and Bhatti [4] investigated the impression of using nanofluids with numerous nanoparticle natures on the thermal properties of a permeable semi-annulus exposed to a uniform magnetic field. They claimed that the platelet form containing nanofluid has the highest heat transfer rate. Even though the Nusselt number enhanced as the volume fraction increased the Darcy and Reynolds numbers decreased as the Lorentz forces increased. Hajabdollahi and Hajabdollahi [5] computationally evaluated the thermo-economic efficiency of a shell-and-tube heat transfer by introducing numerous natures of nanoparticles. The findings revealed that the brick form of nanoparticles gave the best circumstances for thermo-economic performance. Shah et al. [6] investigated the effect of the Atangana-Baleanu time-fractional integral with ternary nanomaterial suspended particles on second-grade fluid crossing an infinite vertical plate. Dawar et al. [7] conducted a theoretical investigation of MHD Jeffrey three-dimensional nanofluid flows with velocity slip conditions on a dual stretched surface. They solve the current flow problem via the HAM for multiple slip constraints and convective heating, using the passive control approach of nanoparticles and non-homogeneous nanofluid model. Gowda et al. [8] described a Casson–Maxwell electrically conducting fluid flow that was restricted through two

consistently stretchable discs. Kumar et al. [9] explored the impacts of thermal radiation and non-uniform heat sink/source influence on nanoliquid flow through a stretchable sheet in the existence of magnetic dipole and chemical reaction. Hossienzadeh et al. [10] explore the thermal efficiency of a moving permeable fin wetted by means of a hybrid nanofluid with distinct cross-sections in the existence of a magnetic field. Hosseinzadeh et al. [11] analysed non-Newtonian martial factors that include nanoparticles in highly permeable vessels. Hosseinzadeh et al. [12] studied the influences of Eckert quantity, volume fraction, and shape factor on the formation of entropy in Bödewadt hybrid three-dimensional flow of nanomaterial with hexanol containing Fe_3O_4 and MoS_2 and base fluids water. Chu et al. [13] investigate heat transfer and flow kinematics from the standpoint of TiO2 and Al2O3 nanoparticles utilised to improve the thermal properties of the base liquids. A significant amount of work has recently been completed [14]–[22].

Carbon nanoparticles have recently attracted the interest of investigators because of their large heat transfer rate. Carbon nanotubes, also known as SWCNTs and MWCNTs, are cylindrical-shaped smooth solids made of a single of several graphene layers. CNTs have made industrial development the largest field of operation by producing thousands of tons of products. CNTs are integrated with polymers and other resources to build structural and composite materials with unique qualities as required by their application and specification, owing to their mechanical properties such as high tensile strength and increased stability. CNTs were used in water flow under the melting heat transfer impacts and homogeneous-heterogeneous reactions by Hayat et al. [23]. For the flow model, two different kinds of CNTs, SWCNT, and MWCNT were included in the water. When MWCNT was dispersed in the base fluid, it was discovered that it had the lowest thermal resistance and highest heat transfer when compared to other nanofluids. Hassanan

et al. [24] studied the oil-CNT flow of nanofluid through stretching sheet, as well as the impact of MHD and radiation. Because of their high thermal conductivity, energy enrichment in oil-SWCNTs was larger than in oil-MWCNTs, while the inclination was the conflicting for velocity profile because of densities modifications. Hayat et al. [25] quantitatively examined the Darcy-Forchheimer flow of CNTs over an exponentially stretched curved surface and discovered that increasing the Forchheimer number has the opposite effect on velocity and temperature profiles. Taseer et al. [26] investigated 3D nanofluid flow including both types of CNTs in a Darcy-Forchheimer porous medium through a nonlinear stretched surface using the optimal series scheme. The stagnation point flow through a stretched sheet was studied by Muhammad et al. [27] using hybrid nanoparticles (CuO and CNTs) and gasoline oil. In their study, they took into account the convective state in conjunction with the viscous dissipation stimulus.The vast uses of heat transfer by a stretchy sheet have piqued the interest of scientists and engineers. Paper, metal spinning, glass, fiber and wire coating, chemical equipment manufacturing, drawing plastic sheets and food manufacturing are just a few of the uses. Crane [28] was the first to commence viscous fluid flow through a stretchy sheet. Rashidi et al. [29] analyzed the heat transfer of an incompressible continuous water-based nanofluid flow through a stretched sheet using thermal radiation in the existence of a transverse magnetic field. They discovered that increasing the buoyancy parameter enhances the velocity of the nanofluid while decreasing its temperature. Turkyilmazoglu [30] investigated the heat transfer in B*ö*dewadt flow on a non-rotating yet stretched disk. His results, in the lack of stretching, revealed a constant temperature all over the viscous boundary layer, and so failed to ensure the thermal field's outer boundary requirement. The flow of nanoliquid generated by a stretching disk was investigated by Mustafa et al. [31].

They came to the conclusion that uniform disk stretching is a key component in reducing boundary layer thickness. A noteworthy work has recently been accomplished [32]– [35].

Eringen [36] was the first to produce micropolar fluid. Micropolar fluid, as stated by them, is a sort of liquid with microscopic influences arising from the micro-motion and local design of fluid molecules. This liquid, which is made up of fluid particles, may both support and stress the body.The important factors in the application of Eringen's micro continuum mechanics incorporate kinematic factors such as the gyration tensor, the microinertia moment tensor, as well as the added ideas of stress moments, body moments, and ordinary micro-stress to the traditional continuum mechanics. Bhargava et al. [37] studied unrestricted convective MHD micropolar fluid between two permeable vertical sheets and found that the velocity drops as the Hartman number increases. Haq et al. [38] considered the impacts of radiation and buoyancy on the micropolar nanofluid stagnation point flow across a vertically convective stretched surface. The micropolar hybrid nanofluid through circular cylinder was researched by Nadeem and Abbas [39]. They used drag force and Nusselt number to emphasize the consequences of various physical phenomena. Abbas et al. [40] inspected the impression of heat radiation and stagnation point MHD flow on micropolar fluid passing over a circular cylinder by means of sinusoidal radius fluctuation. In addition, the impact of porosity and the velocity slip jump is assumed. Alsaadi et al. [41] investigated the entropy optimization in a CNTs (both SWCNTs and MWCNTs) squeezing flow. They used the melting effect to transport heat. Xue [42] considered the transportation mechanism for nanofluids characterized by thermal conductivity. Khan et al. [43] used the HAM to investigate the point flow of a three-dimensional micropolar fluid across a leaky off-centered infinite spinning disk in a permeable material while accounting for Darcy's

confrontation for the micropolar fluid. A substantial quantity of remarkable work has recently been completed [44]–[51].

The main objective of this research is to investigate the three-dimensional micropolar nanofluid in a radiative B*ö*dewadt flow of nanomaterials via a stretched disc. CNTs are deferred in baseliquids such as gasoline oil and water. The Darcy-Forchheimer porous media and viscous dissipation are considered in momentum equation and energy equation, respectively. By employing relevant variables, the governing flow field equations (PDEs) are turned into a system of ordinary differential equations. The bvp4c approach is used for the solution of these ordinary nonlinear differential equations. A brief graphical explanation is provided in a separate section, and the conclusion of relevant material constraints is precisely depicted. As far as we know, nobody has raised this point.

- **Nomenclature**

c_b	Drag coefficient
h	Heat transfer coefficient
j	Micro inertia
$\bar{K}$	Gyro-viscosity
k	Thermal conductivity $(W\ m^{-1}\ K^{-1})$
k^*	Permeability of porous medium (m^2)
N_1, N_2	Angular velocity components for micro-rotation $(m\ s^{-1})$
p	Pressure (pa)
T	Temperature of fluid $(kelvin)$
u, v, w	Velocity components $(m\ s^{-1})$
r, θ, z	Coordinates axis (m)
	Greek Letter
α	Thermal diffusivity (m^2/s)

γ	Micro-rotational coupling coefficient
μ	Dynamic viscosity (kg/ms)
ν	Kinematic viscosity (m^2/s)
ρ	Density $(kg\ m^{-3})$
ρC_p	Heat capacitance
Ω	Uniform angular velocity$(m\ s^{-1})$
σ^*	Stefan Boltzman constant
ϕ	Volume fraction
	Subscript
f	Base fluid
nf	Nanofluid
ω	Wall
∞	Free stream
CNT	Carbon nanotube
SWCNT	Single-Walled Carbon nanotube
MWCNT	Multi-Walled Carbon nanotube

2. Mathematical Formulation

The flow field's controlling physical problem is written in cylindrical coordinates (r, θ, z). The micropoler fluid above the stationary disk is considered to be at $z = 0$. The micropoler fluid motion is caused by the fluid rotating much far ahead from the static disk at a constant angular velocity Ω. Gasoline oil and water are utilized as the foundation liquids. Carbon nanotubes (both SWCNTs and MWCNTs) are ejected from these base liquids. In these base liquids, carbon nanotubes (both SWCNTs and MWCNTs) are suspended. The velocity of fluid flow is $V = (u, v, w)$. In momentum equation the porous medium of Darcy-Forchheimer is taken into account. Heat transport is evaluated by radiation and viscous dissipation. The derivative along

(tangential coordinate) is not taken into account because of axial symmetry flow. The disc is also linearly enlarged in the radial direction at a uniform rate c (see Fig. 1).

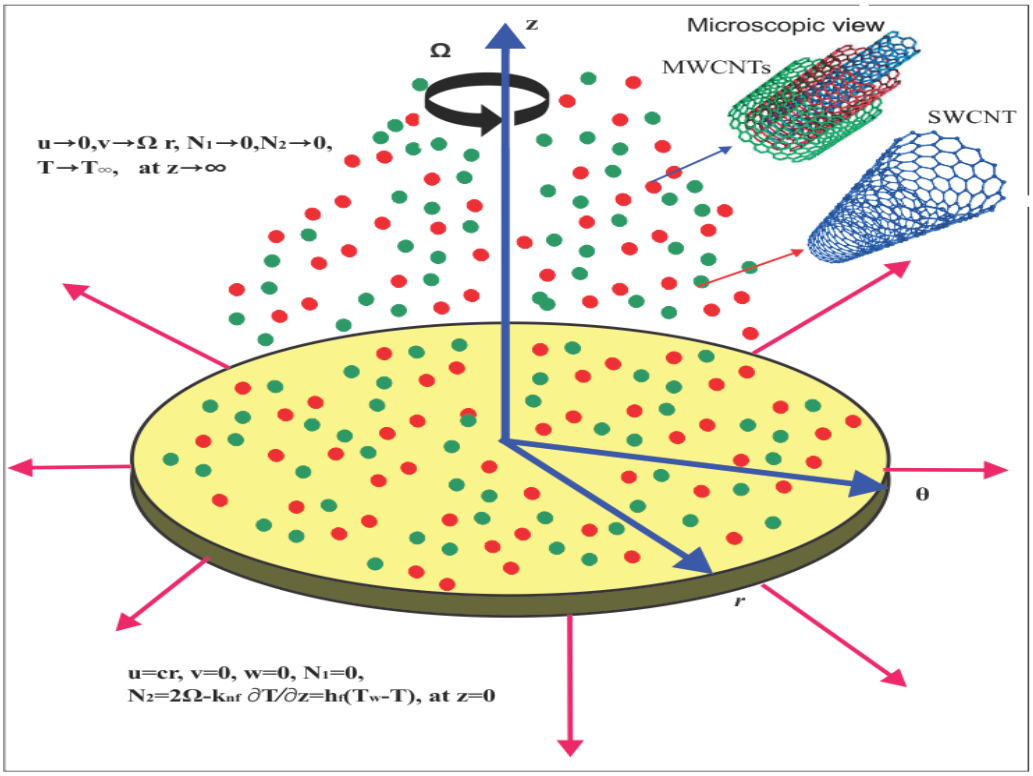

Fig.1 Geometry of the flow problem

Under these assumptions continuity, momentum, energy and nanoparticle volume fraction of the microrotation vector is given as [28, 30]:

$$\frac{\partial u}{\partial r}+\frac{u}{r}+\frac{\partial w}{\partial z}=0 \tag{1}$$

$$u\frac{\partial u}{\partial r}-\frac{v^2}{r}+w\frac{\partial u}{\partial z}=-\frac{1}{\rho_{nf}}\frac{\partial p}{\partial r}+\frac{(\mu_{nf}+\mathbb{K})}{\rho_{nf}}\left(\frac{\partial^2 u}{\partial r^2}+\frac{1}{r}\frac{\partial u}{\partial r}-\frac{u}{r^2}+\frac{\partial^2 u}{\partial z^2}\right) -\frac{\mathbb{K}}{\rho_{nf}}\frac{\partial N_2}{\partial z}-\frac{1}{\rho_{nf}}\frac{\mu_{nf}}{k^*}u+Fu^2 \tag{2}$$

$$u\frac{\partial v}{\partial r}-\frac{uv}{r}+w\frac{\partial v}{\partial z}=\frac{(\mu_{nf}+\mathbb{K})}{\rho_{nf}}\left(\frac{\partial^2 v}{\partial r^2}+\frac{1}{r}\frac{\partial v}{\partial r}-\frac{v}{r^2}+\frac{\partial^2 v}{\partial z^2}\right)-\frac{\mathbb{K}}{\rho_{nf}}\frac{\partial N_1}{\partial z}-\frac{1}{\rho_{nf}}\frac{\mu_{nf}}{k^*}v+Fv^2 \tag{3}$$

$$u\frac{\partial N_1}{\partial r}-\frac{vN_2}{r}+w\frac{\partial N_1}{\partial z}=\frac{\gamma}{j\rho_{nf}}\left(\frac{\partial^2 N_1}{\partial r^2}+\frac{1}{r}\frac{\partial N_1}{\partial r}-\frac{N_1}{r^2}+\frac{\partial^2 N_1}{\partial z^2}\right)-\frac{\mathbb{K}}{j\rho_{nf}}\left(\frac{\partial v}{\partial z}+2N_1\right) \quad (4)$$

$$u\frac{\partial N_2}{\partial r}-\frac{vN_1}{r}+w\frac{\partial N_2}{\partial z}=\frac{\gamma}{j\rho_{nf}}\left(\frac{\partial^2 N_2}{\partial r^2}+\frac{1}{r}\frac{\partial N_2}{\partial r}-\frac{N_2}{r^2}+\frac{\partial^2 N_2}{\partial z^2}\right)-\frac{\mathbb{K}}{j\rho_{nf}}\left(\frac{\partial u}{\partial z}-\frac{\partial w}{\partial r}-2N_2\right) \quad (5)$$

$$u\frac{\partial T}{\partial r}+w\frac{\partial T}{\partial z}=\alpha_{nf}\left(\frac{\partial^2 T}{\partial r^2}+\frac{1}{r}\frac{\partial T}{\partial r}+\frac{\partial^2 T}{\partial z^2}\right)-\frac{16\sigma^* T_\infty^3}{(\rho c_p)_{nf}k_1^*}\frac{\partial^2 T}{\partial z^2}+\frac{(\mu_{nf}+\mathbb{K})}{(\rho c_p)_{nf}}\left(2\left(\frac{u}{r}\right)^2+\left(\frac{\partial v}{\partial z}\right)^2+\left(\frac{\partial w}{\partial z}\right)^2-\right.$$

$$\left.\frac{v}{r}\left(\frac{\partial v}{\partial r}-\frac{v}{r}\right)+\frac{\partial v}{\partial r}\left(\frac{\partial v}{\partial r}-\frac{v}{r}\right)+\frac{\partial u}{\partial z}\left(\frac{\partial u}{\partial z}-\frac{\partial w}{\partial r}\right)+\frac{\partial u}{\partial r}\left(\frac{\partial u}{\partial z}-\frac{\partial w}{\partial r}\right)\right) \quad (6)$$

The boundary conditions are

$$\begin{aligned} u=cr, v=0, w=0, N_1=0, N_2=2\Omega, -k_{nf}\frac{\partial T}{\partial z}=h_f(T_\omega-T) \quad at \quad z=0 \\ u\to 0, v\to r\Omega, N_1\to 0, N_2\to 0, T\to T_\infty \qquad at \qquad z\to 0 \end{aligned} \quad (7)$$

Newton's law of cooling and Fourier's law of heat conduction are used to construct the condition $-k_{nf}\frac{\partial T}{\partial z}=h_f(T_\omega-T)$ at $z=0$ (convective boundary condition). Physically, in the described state, heated fluid is pumped beneath the disk, acting as a heat source via convection and conduction. Also $F=\frac{c_b}{\sqrt{k^*}r}$ is non-uniform inertia factor.

At frictionless conditions, the centrifugal acceleration balances and radial pressure gradient out of [36]:

$$\frac{1}{\rho_{nf}}\frac{\partial p}{\partial r}=r\Omega^2 \quad (8)$$

The Xue theoretical model employs the terms [42]:

$$\mu_{nf} = \frac{\mu_f}{(1-\phi)^{2.5}},\ \rho_{nf} = (1-\phi)\rho_f + \phi\rho_{CNT},\ \nu_{nf} = \frac{\mu_{nf}}{\rho_{nf}}$$
$$\alpha_{nf} = \frac{k_{nf}}{(\rho c_p)_{nf}},\ \frac{k_{nf}}{k_f} = \frac{(1-\phi)+2\phi\frac{k_{CNT}}{k_{CNT}-k_f}ln\frac{k_{CNT}}{k_{CNT}-k_f}}{(1-\phi)+2\phi\frac{k_f}{k_{CNT}-k_f}ln\frac{k_{CNT}}{k_{CNT}-k_f}} \tag{9}$$

Table 1: Nanoparticle and baseliquid thermal properties [31]:

"Physical features"	"CNTs"		"Baseliquids"	
	"Single-walled"	"Multiple- Walled"	"Water"	"Gasoline Oil"
$\rho\left(\frac{kg}{m^3}\right)$	2600	1600	783	750
$c_p\left(\frac{J}{kgK}\right)$	425	796	2040	2100
$k\left(\frac{W}{mK}\right)$	6600	3000	0.145	1.5
Pr			6.2	9.4

The dimensionless transformation can be defined as follow [43]:

$$\xi = \sqrt{\frac{\Omega}{\nu_f}}z, u = r\Omega f(\xi), v = r\Omega g(\xi), w = \sqrt{\Omega\nu_f}h(\xi), N_1 = \Omega\sqrt{\frac{\Omega}{\nu_f}}rL(\xi),$$
$$N_2 = \Omega\sqrt{\frac{\Omega}{\nu_f}}rM(\xi), \theta(\xi) = \frac{T-T_\infty}{T_\omega-T_\infty}, p(\xi) = \frac{p-p_\infty}{\Omega\rho_f\nu_f} \tag{10}$$

Employing the dimensionless transformation (10), eqs. (1) to (7) becomes

$$h' + 2f = 0 \tag{11}$$

$$\left(\frac{1+(1-\phi)^{2.5}K}{(1-\phi)^{2.5}}\right)f'' - \left(1-\phi+\phi\frac{\rho_{CNT}}{\rho_f}\right)(g^2 - f^2 - hf' - 1 - F_r f^2)$$
$$-\left(\frac{\lambda f}{(1-\phi)^{2.5}} + KM'\right) = 0 \tag{12}$$

$$\left(\frac{1+(1-\phi)^{2.5}K}{(1-\phi)^{2.5}}\right)g'' - \left(\frac{\lambda g}{(1-\phi)^{2.5}} + KL'\right) - \left(1-\phi+\phi\frac{\rho_{CNT}}{\rho_f}\right)(hg' - 1 - F_r g^2) = 0 \tag{13}$$

$$L'' - \frac{\alpha_2}{\alpha_1}(g' + 2L) - \frac{1}{\alpha_1}\left(1-\phi+\phi\frac{\rho_{CNT}}{\rho_f}\right)(fL - Mg + hL') = 0 \tag{14}$$

$$M'' - \frac{\alpha_2}{\alpha_1}(f' + 2M) - \frac{1}{\alpha_1}\left(1 - \phi + \phi\frac{\rho_{CNT}}{\rho_f}\right)(fM - gL + hM') = 0 \tag{15}$$

$$\left(\frac{k_{nf}}{k_f} + \frac{4}{3}Rd\right)\theta'' - \left(1 - \phi + \phi\frac{(\rho c_p)_{CNT}}{(\rho c_p)_f}\right)\Pr h\,\theta' + \Pr Ec\left(\frac{1}{(1-\phi)^{2.5}} + K\right)\left(2f^2 + Re\left(g'^2 + f'^2\right) + h'^2\right) = 0 \tag{16}$$

With boundary constraints

$$h = 0, f = R, g = 0, L = 0, M = 2(Re)^{-1/2}, \theta' = -\frac{\beta}{(k_{nf}/k_f)}(1 - \theta)\ \ at\ \ \xi = 0$$
$$f \to 0, g \to 1, L \to 0, M \to 0, \theta \to 0\ \ at\ \ \xi \to \infty \tag{17}$$

Where $\lambda = \frac{\nu_f}{k^*\Omega}$ is porosity parameter, $F_r = \frac{c_b}{\sqrt{k^*}}$ is Forchheimer number, $K = \frac{\kappa}{\mu_f}$ is vortex viscosity parameter, $\alpha_1 = \frac{\gamma}{\mu_f j}$ is spin gradient viscosity parameter, $\alpha_2 = \frac{\kappa}{\rho_f j\Omega}$ is microinertia density parameter, $Pr = \frac{\nu_f}{\alpha_f}$ is prandtl number, $Ec = \frac{\nu_f\Omega}{T_\omega - T_\infty}$ is Eckert number, $Rd = \frac{4\sigma^* T_\infty^3}{k^* k_f}$ is radiation parameter, $Re = \frac{r^2\Omega}{\nu_f}$ is Reynold number, $R = \frac{c}{\Omega}$ is rotational parameter, and $\beta = \frac{h_f}{k_f}\sqrt{\frac{\nu_f}{\Omega}}$ is thermal Biot number.

3. Parameter of Engineering Interest

The following expressions yield the skin friction coefficient and the Nusselt number, which are discussed in this problem.

$$C_f = \frac{\sqrt{\tau_{rz}^2 + \tau_{\theta z}^2}}{\rho_f (r\Omega)^2},\ Nu_r = \frac{r q_\omega}{k_f(T_\omega - T_\infty)} \tag{18}$$

The radial shear stress τ_{rz}, tangential shear stress $\tau_{\theta z}$, and heat flux $q_\omega$are defined by

$$\tau_{rz} = \left[\left(\mu_{nf} + k\right)\frac{\partial u}{\partial z} + kN_2\right]_{z=0}, \tau_{\theta z} = \left[\left(\mu_{nf} + k\right)\frac{\partial v}{\partial z} + kN_1\right]_{z=0}, q_{\omega} = -k_{nf}\left(\frac{\partial T}{\partial z}\right)_{z=0} \quad (19)$$

The dimensionless skin friction and Nusselt number are as follow:

$$C_f Re = \sqrt{\left(\left(\frac{1+(1-\phi)^{2.5}K}{(1-\phi)^{2.5}}\right)f'(0) + KM(0)\right)^2 + \left(\left(\frac{1+(1-\phi)^{2.5}K}{(1-\phi)^{2.5}}\right)g'(0) + KL(0)\right)^2} \quad (20)$$

$$Nu_r(Re)^{-1/2} = -\frac{k_{nf}}{k_f}\theta'(0) \quad (21)$$

4. Results and Discussion

Graphs depict the influence of several physical constraints like the nanoparticle volume fraction parameter ϕ, rotational parameter R, porosity parameter λ, and vortex viscosity parameter K. Figs. 2-7 show the impacts of axial velocity $h(\xi)$, radial velocity $f(\xi)$, tangential velocity $g(\xi)$, micro rotational velocities $L(\xi)$ and $M(\xi)$ as well as temperature of the fluid $\theta(\xi)$ when nanoparticle volume fraction parameter ϕ is increased. An escalation in ϕ causes a diminution in the tangential and radial velocity components as well as temperature distribution, while the axial component of velocity, micro-rotational velocity of the fluid show the opposite tendency. Multiple-walled CNTs are also more effective than single-walled CNTs, according to research. When compared to water-based fluids, gasoline oil also displays an overarching trend.

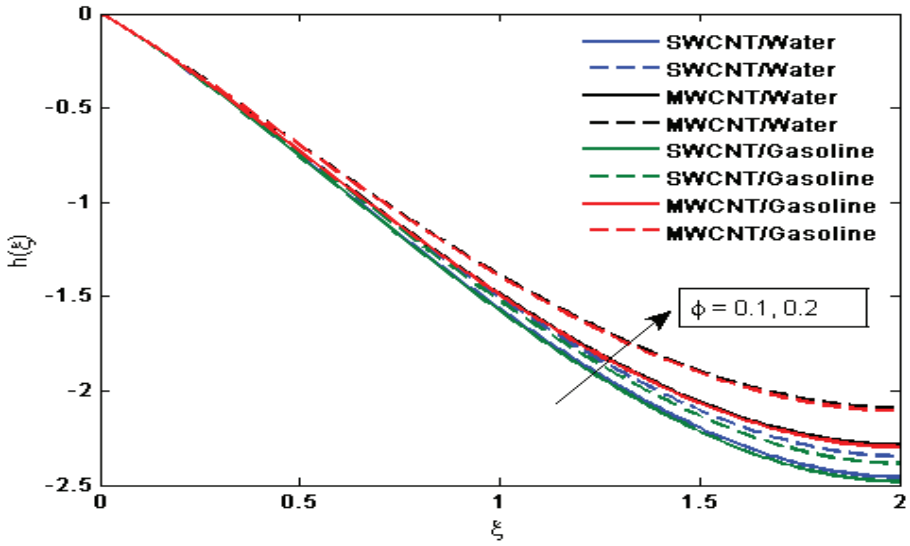

Fig. 2 Influence of ϕ on axial velocity $h(\xi)$ when $F_r = 0.4, K = 0.7, and\ \lambda = 0.5$.

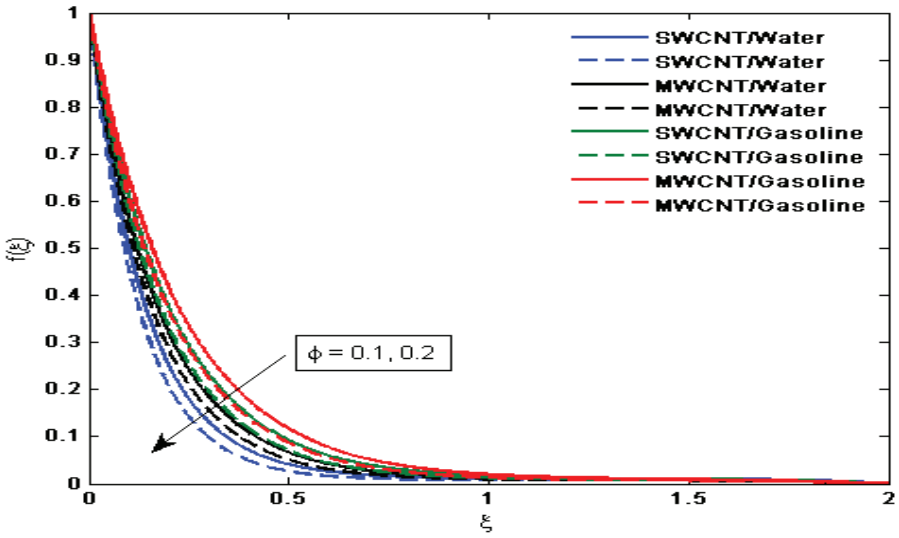

Fig. 3 Influence of ϕ on redial velocity $f(\xi)$ when $F_r = 0.4, K = 0.7, and\ \lambda = 0.5$.

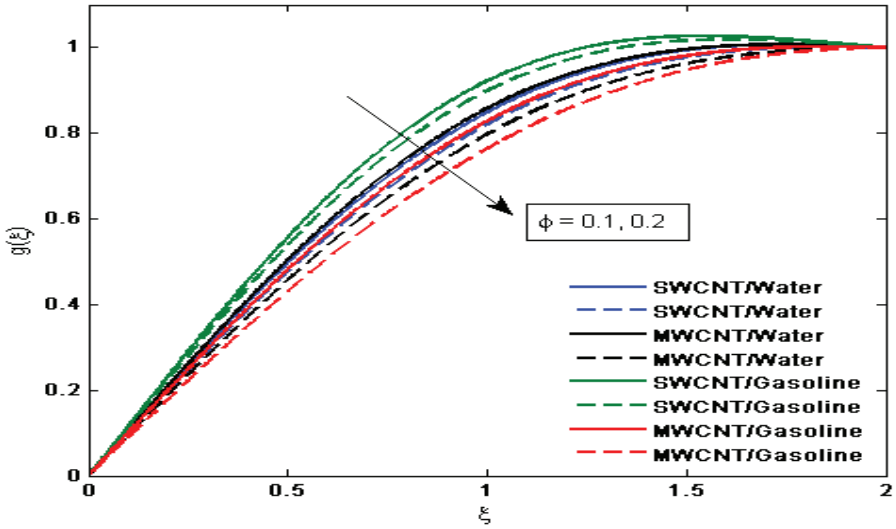

Fig. 4 Influence of ϕ on tangential velocity $g(\xi)$ when $F_r = 0.4, K = 0.7, and\ \lambda = 0.5$.

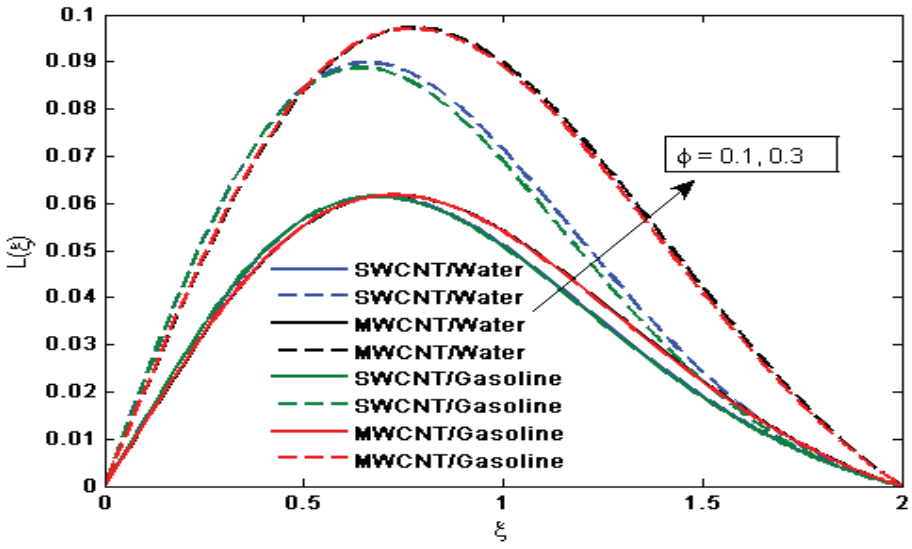

Fig. 5 Influence of ϕ on microrotational velocity $L(\xi)$ when $F_r = 0.4, K = 0.7, \alpha_1 = 0.2, \alpha_2 = 0.1, and\ \lambda = 0.5$.

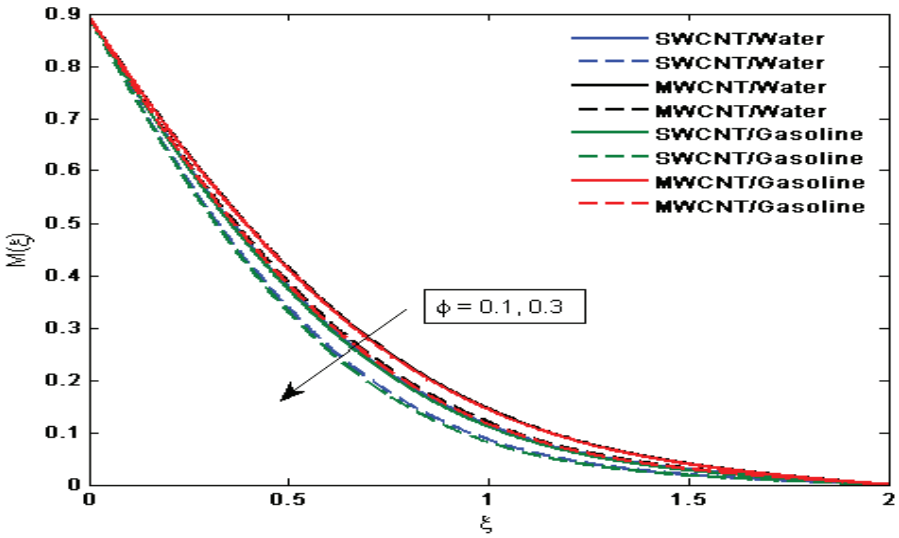

Fig. 6 Influence of ϕ on microrotational velocity $M(\xi)$ when $F_r = 0.4, K = 0.7, \alpha_1 = 0.2, \alpha_2 = 0.05, and\ \lambda = 0.5$.

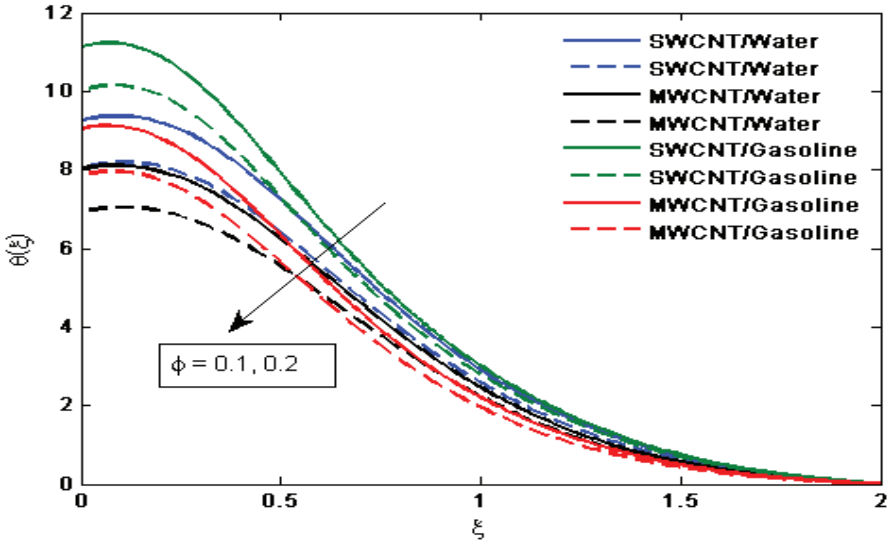

Fig. 7 Influence of ϕ on temperature profile $\theta(\xi)$ when $F_r = 0.4, K = 0.7, \lambda = 0.5, Ec = 1.2, Rd = 0.4, and\ Re = 0.2$.

Figs. 8-13 show the components of velocity (flow), micro-rotational velocities and temperature as R enhances. It is observed that the tangential and radial velocities as well as temperature increases by increasing the value of R while opposite behavior are observed for axial component of velocity and micro-rotational velocities. Because R is the ratio of stretching rate to rotational rate, increasing R induces considerable surface stretching, resulting in a fluid rise due to the no-slip requirement. More hot fluid will be transported from the surface to the cold fluid, intensifying the temperature field. Moreover, multiple-walled CNTs have a greater behavior than single-walled CNTs. It's worth noting that gasoline oil-based fluid takes precedence over water-based fluid.

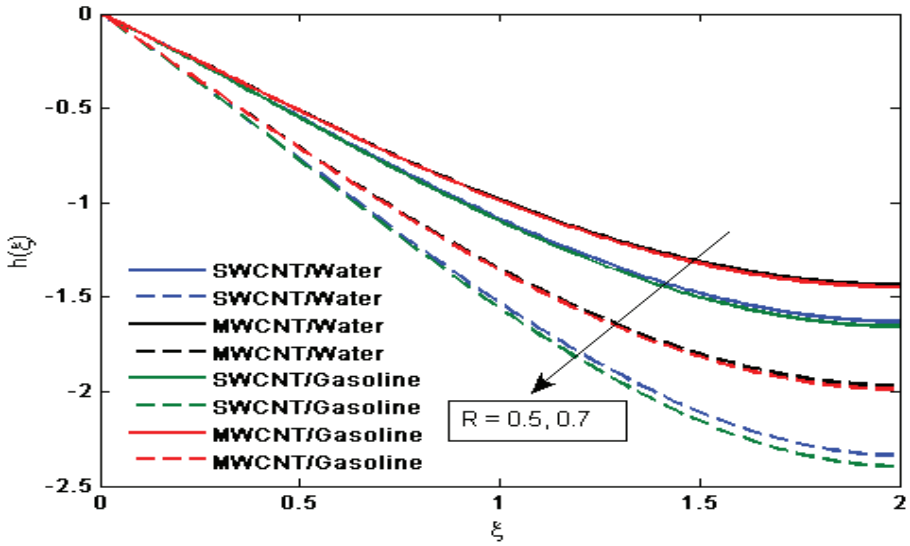

Fig. 8 *Influence of* R *on axial velocity* $h(\xi)$ *when* $F_r = 0.4,\ \phi = 0.1, K = 0.7, and\ \lambda = 0.5$.

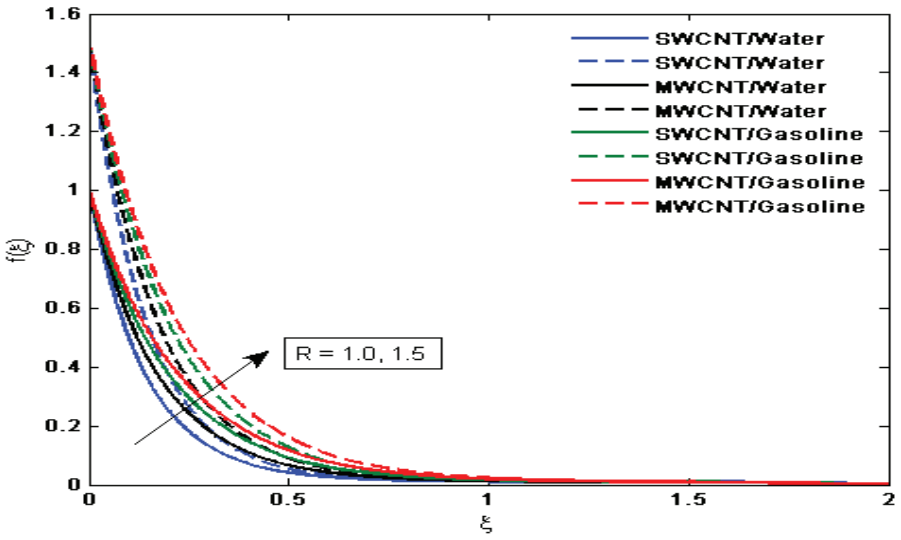

Fig.9 Influence of R on redial velocity $f(\xi)$ *when* $F_r = 0.4,\ \phi = 0.1, K = 0.7,$ *and* $\lambda = 0.5$.

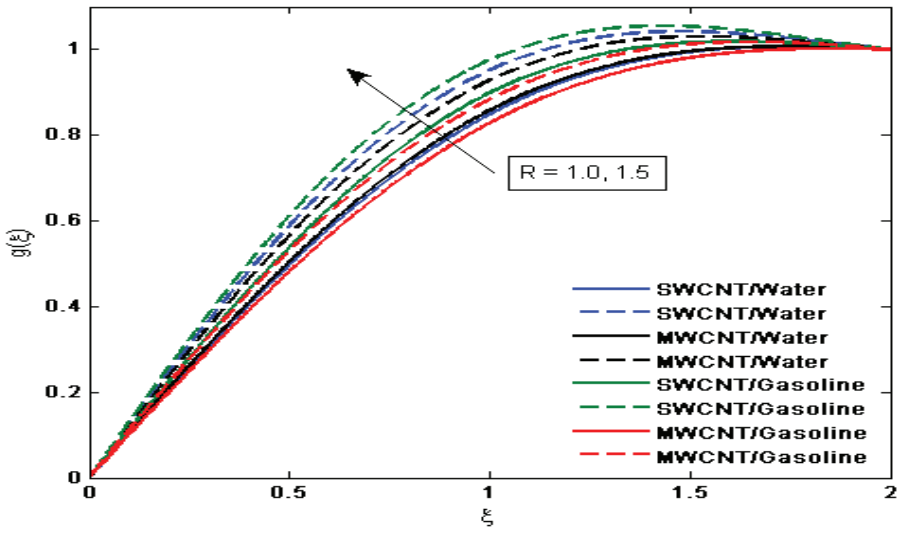

Fig.10 Influence of R on tangential velocity $g(\xi)$*when* $F_r = 0.4,\ \phi = 0.1, K = 0.7, and\ \lambda = 0.5$.

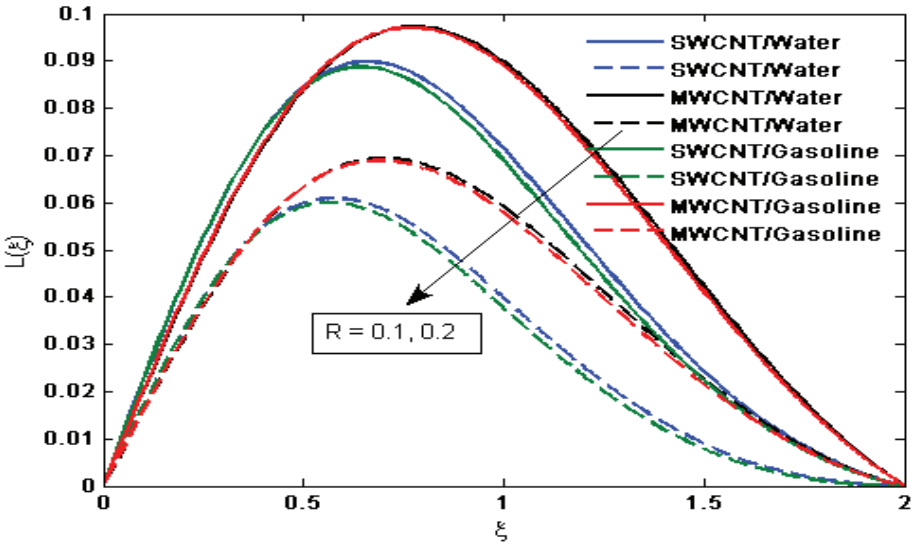

Fig. 11 *Influence of* R *on microrotational velocity* $L(\xi)$ *when* $F_r = 0.4,\ \phi = 0.1, \alpha_1 = 0.2, \alpha_2 = 0.1, K = 0.7, and\ \lambda = 0.5.$

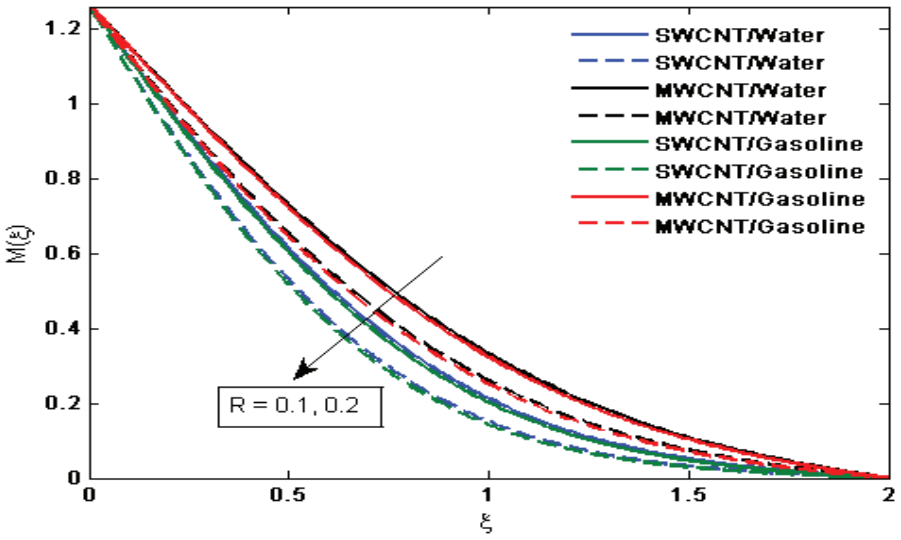

Fig. 12 *Influence of* R *on microrotational velocity* $M(\xi)$ *when* $F_r = 0.4,\ \phi = 0.1, \alpha_1 = 0.2, \alpha_2 = 0.05, K = 0.7, and\ \lambda = 0.5.$

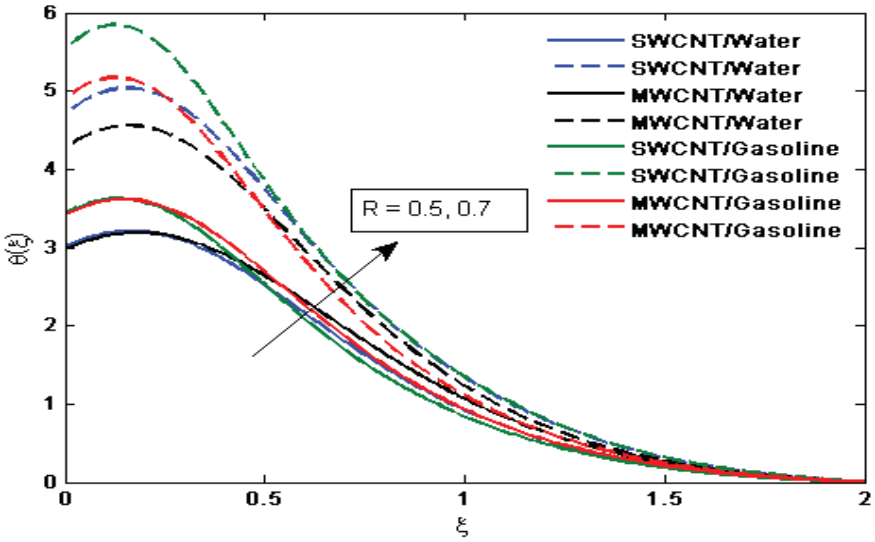

Fig. 13 *Influence of R on temperature profile* $\theta(\xi)$ *when* $F_r = 0.4,\ \phi = 0.1, K = 0.7, Ec = 1.2, Rd = 0.4, Re = 0.2, and\ \lambda = 0.5.$

Figs. 14-19 depict how λ changes fluid velocity, micro-rotational velocities and temperature fields. The radial, tangential velocity and temperature of the fluid decay with rise in λ, however axial velocity and micro-rotational velocity rise with raise in λ. Physically, an increase in λ provided more porous space, which provided opposition to fluid movement. As a result, the flow field becomes smaller. Multiple-walled CNTs are preferred over single-walled CNTs, and gasoline over water-based fluid is preferred.

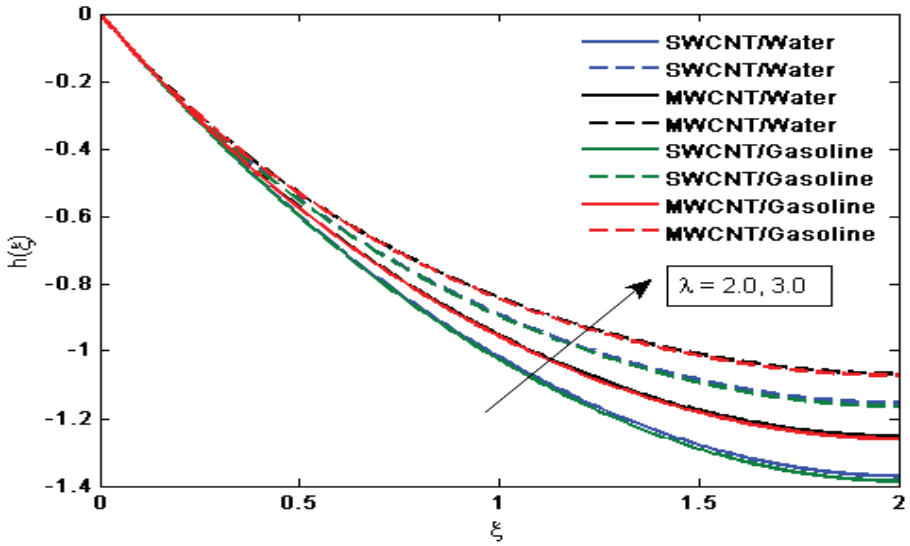

Fig. 14 *Influence of* λ *on axial velocity* $h(\xi)$ *when* $F_r = 0.4,\ \phi = 0.1, and\ K = 0.7.$

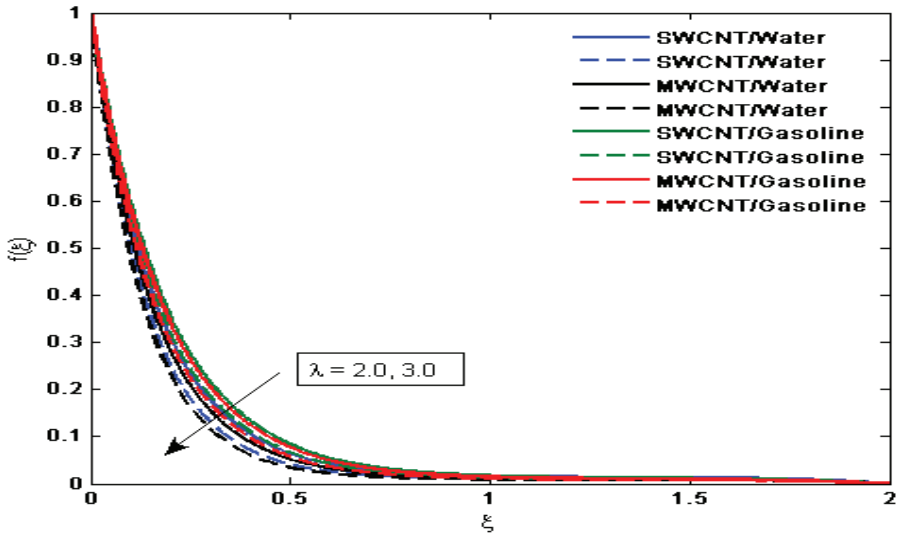

Fig. 15 *Influence of* λ *on redial velocity* $f(\xi)$*when* $F_r = 0.4,\ \phi = 0.1, and\ K = 0.7.$

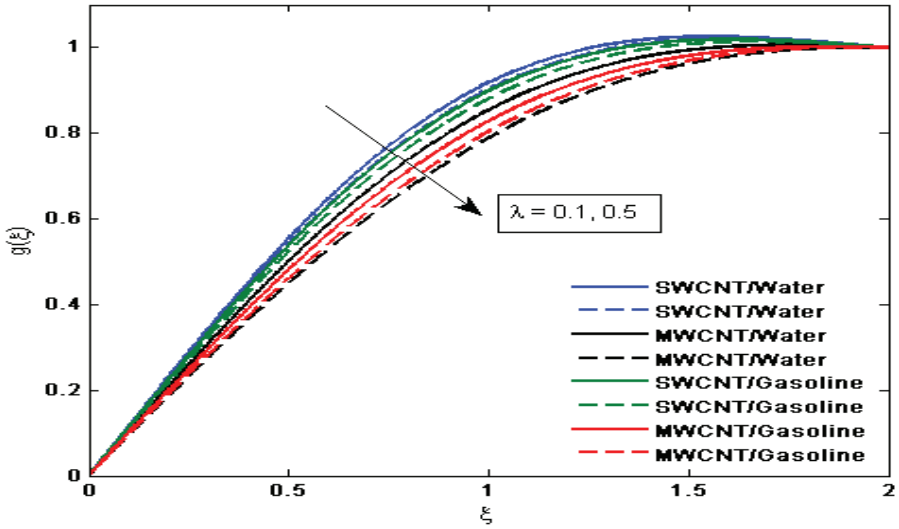

Fig. 16 *Influence of* λ *on tangential velocity* $g(\xi)$ *when* $F_r = 0.4,\ \phi = 0.1, and\ K = 0.7.$

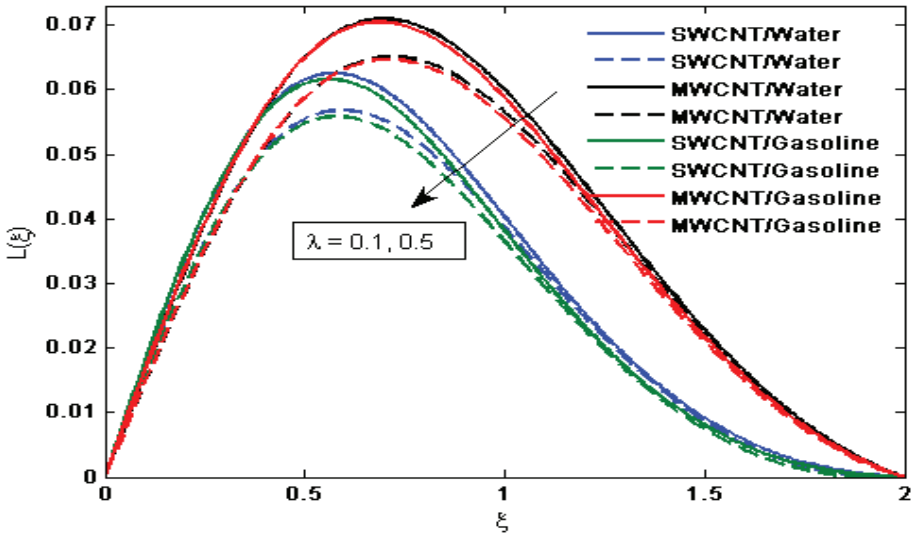

Fig. 17 *Influence of* λ *on microrotational velocity* $L(\xi)$ *when* $F_r = 0.4,\ \phi = 0.1, \alpha_1 = 0.2, \alpha_2 = 0.1, and\ K = 0.7.$

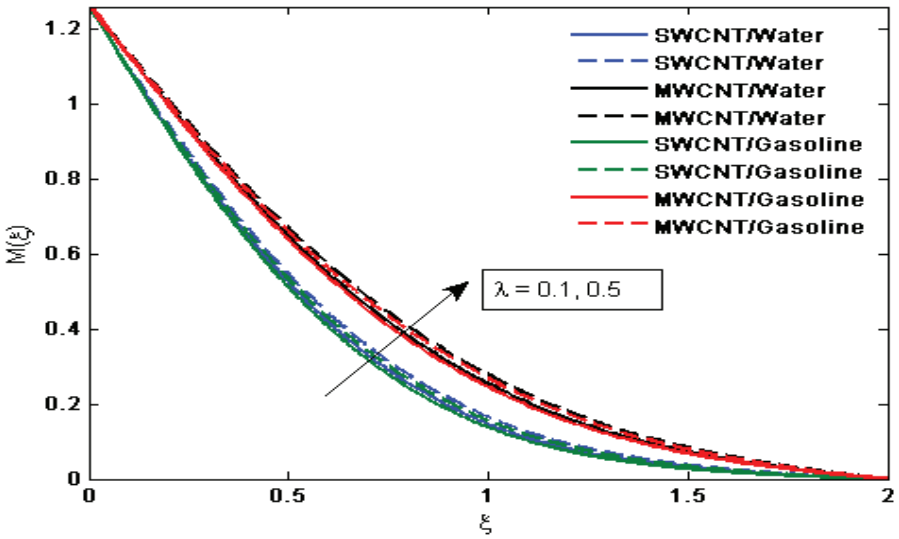

Fig. 18 *Influence of* λ *on microrotational velocity* $M(\xi)$ *when* $F_r = 0.4,\ \phi = 0.1, \alpha_1 = 0.2, \alpha_2 = 0.05,$ *and* $K = 0.7.$

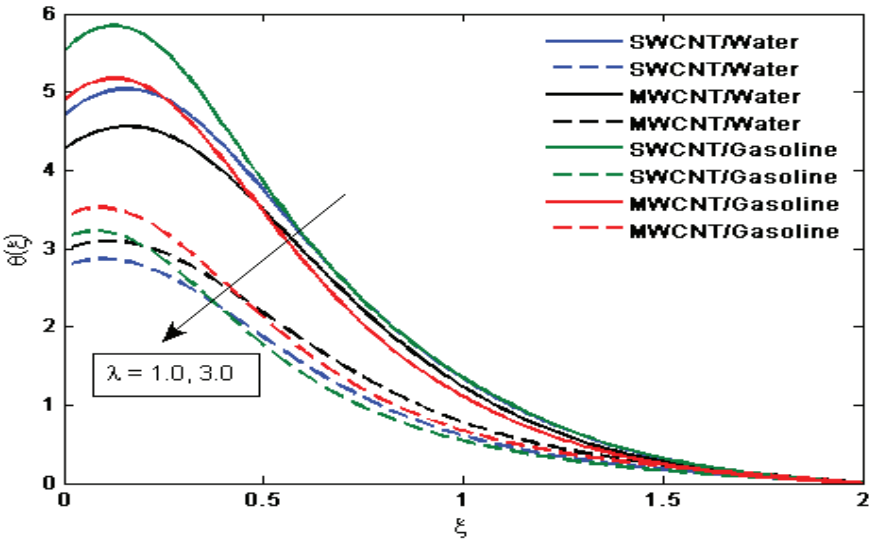

Fig. 19 *Influence of* λ *on temperature profile* $\theta(\xi)$ *when* $F_r = 0.4,\ \phi = 0.1, Ec = 1.2, Rd = 0.4, Re = 0.2,$ *and* $K = 0.7.$

Figs. 20-25 shows how the material parameter of fluid effects on velocity and temperature. Raising the values of fluid parameter causes the radial velocity component and temperature to rise, but the axial, tangential, and micro rotational velocity components have the reverse effect.

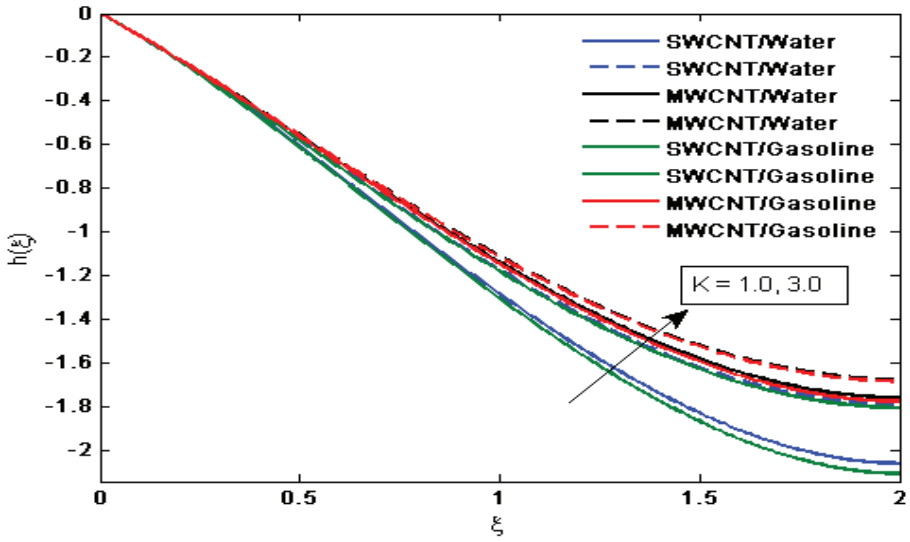

Fig. 20 *Influence of* K *on axial velocity* $h(\xi)$ *when* $F_r = 0.4,\ \phi = 0.1, and\ \lambda = 0.5.$

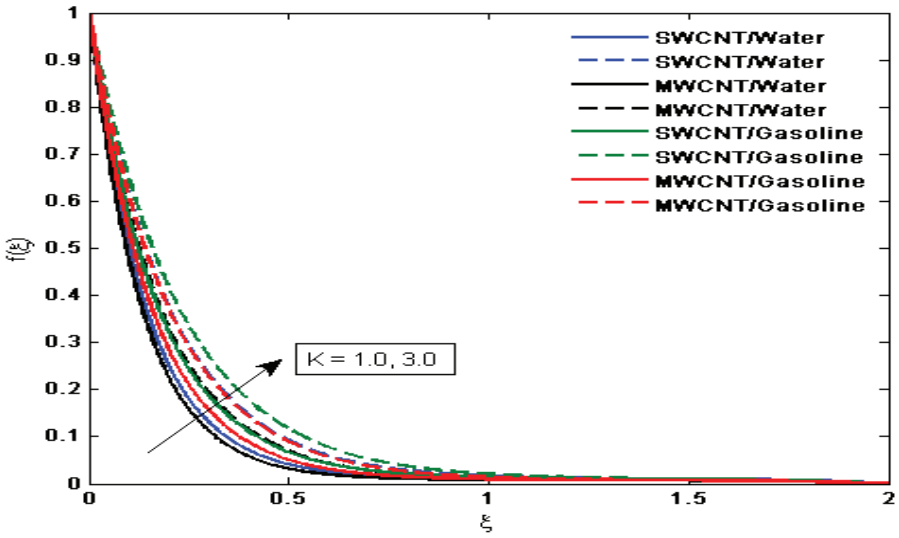

Fig. 21 *Influence of* K *on redial velocity* $f(\xi)$ *when* $F_r = 0.4,\ \phi = 0.1, and\ \lambda = 0.5.$

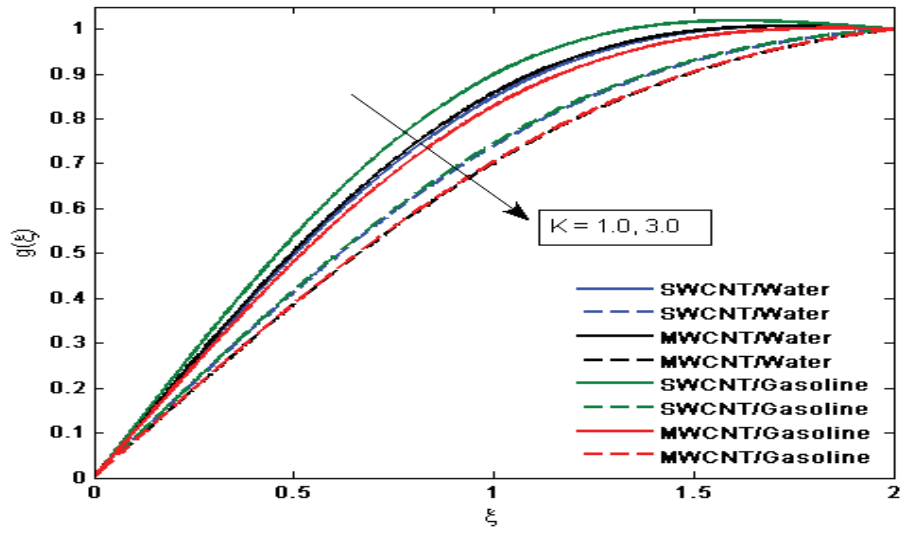

Fig. 22 Influence of K on tangential velocity $g(\xi)$ *when* $F_r = 0.4,\ \phi = 0.1,$ *and* $\lambda = 0.5.$

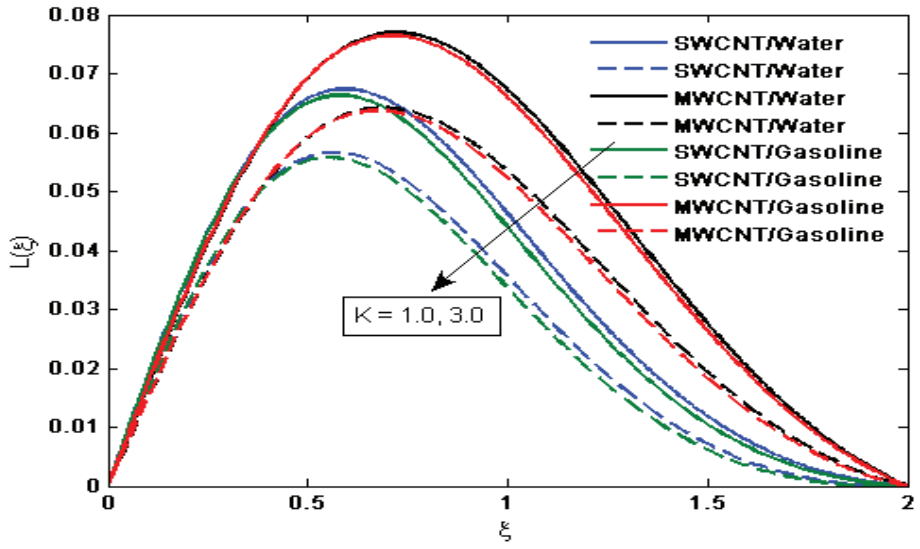

Fig. 23 Influence of K on microrotational velocity $L(\xi)$ *when* $F_r = 0.4,\ \phi = 0.1, \alpha_1 = 0.2, \alpha_2 = 0.1,$ *and* $\lambda = 0.5.$

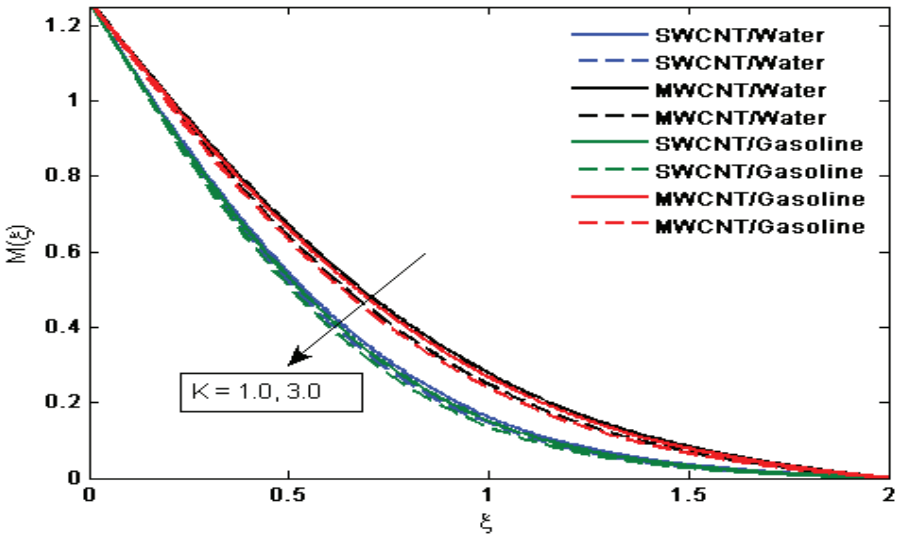

Fig. 24 Influence of K on microrotional velocity $M(\xi)$ *when* $F_r = 0.4,\ \phi = 0.1, \alpha_1 = 0.2, \alpha_2 = 0.05,$ *and* $\lambda = 0.5.$

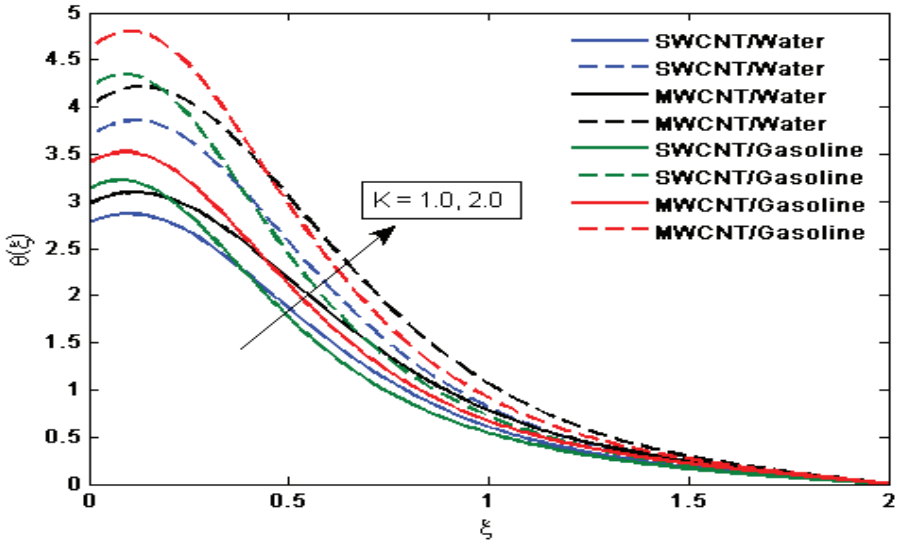

Fig. 25 Influence of K on temperature profile $\theta(\xi)$ *when* $F_r = 0.4,\ \phi = 0.1, Ec = 1.2, Rd = 0.4, Re = 0.2,$ *and* $\lambda = 0.5.$

Figs. 26-27 exhibit the trend of the spin gradient viscosity factor α_1 on micro-rotational profile $L(\xi)$ and $M(\xi)$. The rising values of spin gradient viscosity factor increased the micro-rotational velocities $L(\xi)$ and $M(\xi)$.

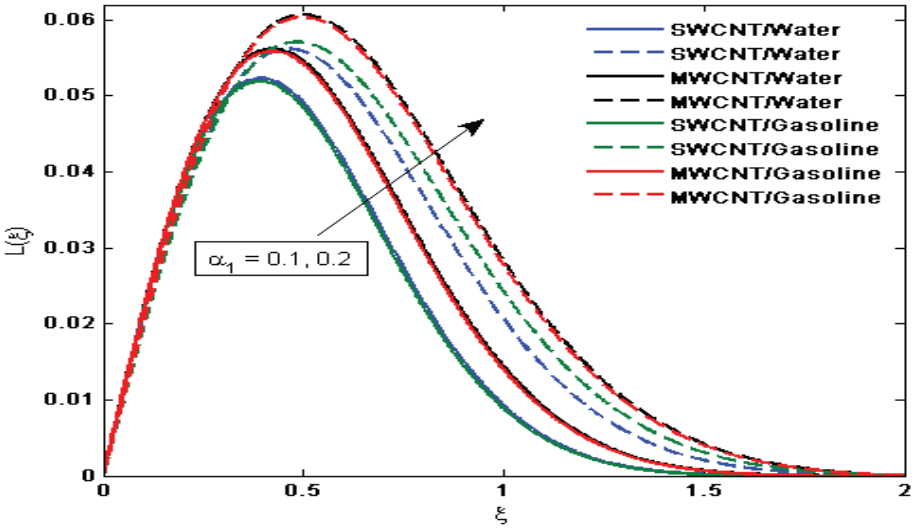

Fig. 26 Influence of α_1 on microrotational velocity $L(\xi)$ when $F_r = 0.4,\ \phi = 0.1, \alpha_2 = 0.2, K = 0.7, and\ \lambda = 0.5$.

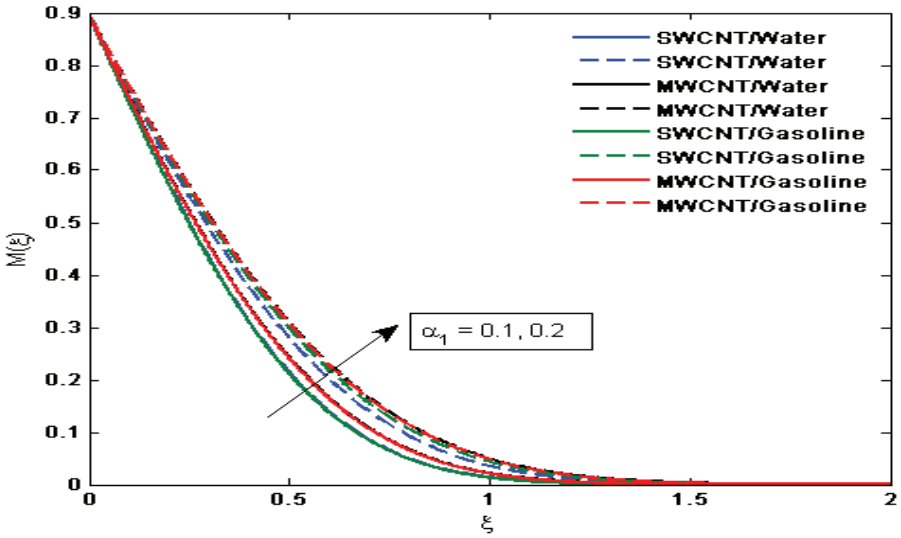

Fig. 27 Influence of α_1 *on microrotational velocity* $M(\xi)$*when* $F_r = 0.4,\ \phi = 0.1, \alpha_2 = 0.05, K = 0.7, and\ \lambda = 0.5.$

Figs. 28-29 show the consequence of the micro-inertia density factor α_2 on the micro-rotational velocities $L(\xi)$ and $M(\xi)$. The enhancement of the micro-inertia density constraint shows that $L(\xi)$ decline, while $M(\xi)$ rise up. It was also found from figs. 26-27 and figs. 28-29 that the effect of multiple-walled CNTs is quite effective than that of single-walled CNTs. When compared to water-based fluids, gasoline oil also displays an overarching trend.

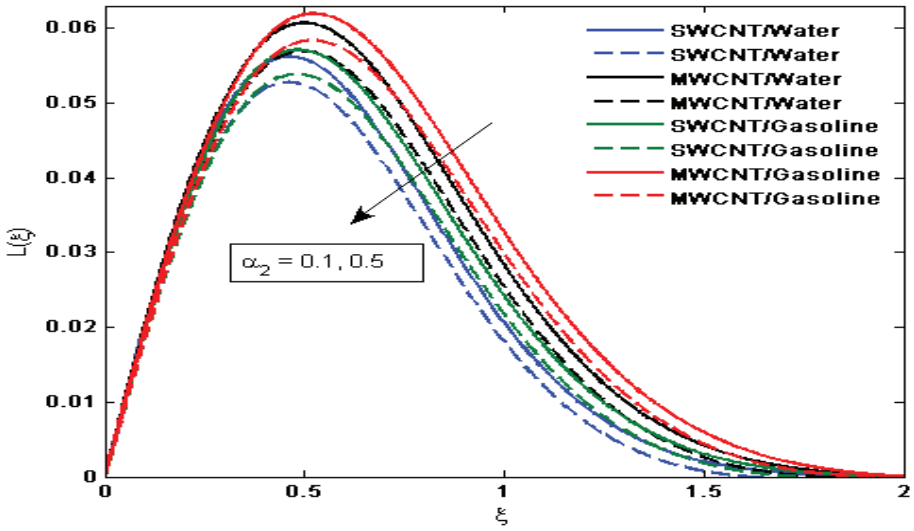

Fig. 28 Influence of α_2 *on microrotational velocity* $L(\xi)$ *when* $F_r = 0.4,\ \phi = 0.1, K = 0.7, \alpha_1 = 0.2, and\ \lambda = 0.5.$

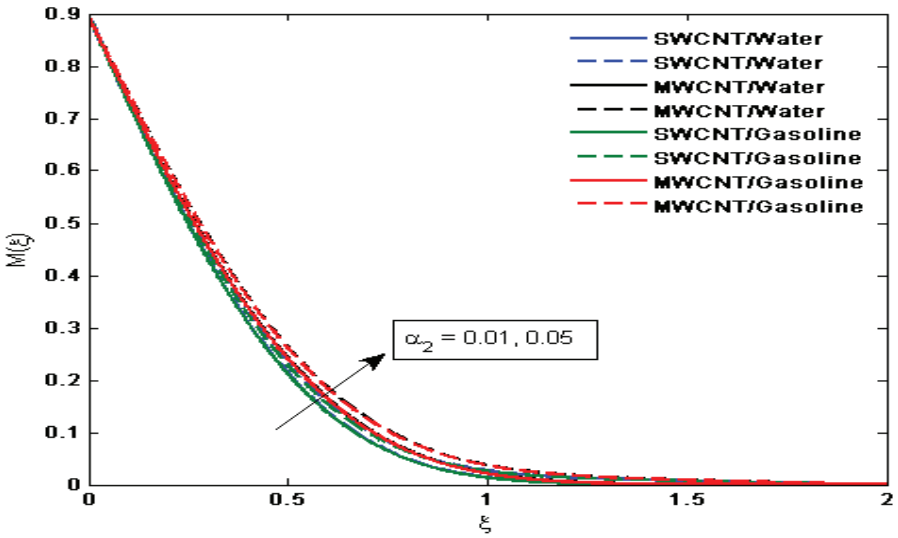

Fig. 29 Influence of α_2 *on microrotational velocity* $M(\xi)$ *when* $F_r = 0.4,\ \phi = 0.1, K = 0.7, \alpha_1 = 0.2,$ *and* $\lambda = 0.5$.

Table 2 demonstrates the variation in the skin friction coefficient for numerous values of $\phi, R, \lambda,$ and K. Observing from the table, skin friction decay when the volume fraction ϕ and porosity parameter λ rise up, while skin friction upsurges for rising values of rotational parameter R and vortex viscosity parameter K.

Table 2: Illustrate the influence of numerous parameters on skin fraction coefficient.

ϕ	R	λ	K	SWCNT/Water	MWCNT/Water	SWCNT/Gasoline	MWCNT/Gasoline
0.1	0.5	1.0	1	5.73921	4.21211	4.96473	4.26111
0.2				4.76347	3.77399	4.95695	3.82743
0.3				4.29721	3.37586	4.42414	3.43311
0.1	0.1			3.80377	3.60713	3.827	3.62061
	0.3			4.028	3.70841	4.06866	3.72924
	0.5			5.73921	4.21211	4.96473	4.26111
0.1	0.5	1.0		5.73921	4.21211	4.96473	4.26111
		2.0		3.29009	2.97347	3.32963	2.99435

		3.0		2.4931	2.27118	2.5195	2.28632
			1.0	2.4931	2.27118	2.5195	2.28632
			2.0	7.29044	6.75265	7.36016	6.7873
			3.0	9.8482	9.3664	9.9059	9.39919

Table 3 shows how the Nusselt number varies for various values of ϕ, R, λ, and K. Nusselt number increases with increasing values of volume fraction ϕ and porosity parameter λ, but decreases with increasing values of rotational parameter R and vortex viscosity parameter K, as seen in the table. It was also revealed that multiple-walled CNTs had a greater impact than single-walled CNTs. When compared to water-based fluids, gasoline oil follows a similar pattern.

Table 3: Illustrate the influence of numerous parameters on Nusselt number.

ϕ	R	λ	K	SWCNT/Water	MWCNT/Water	SWCNT/Gasoline	MWCNT/Gasoline
0.1	0.5	1.0	1.0	-6.66911	-4.50457	-5.74297	-5.16785
0.2				-4.25552	-3.69728	-5.01863	-4.23932
0.3				-3.44051	-3.32393	-3.9513	-3.81609
	0.1			-2.15637	-2.10379	-2.47961	-2.42477
	0.3			-3.05381	-2.91	-3.49807	-3.32861
	0.5			-6.66911	-4.50457	-5.74297	-5.16785
0.1	0.5	1.0		-6.66911	-4.50457	-5.74297	-5.16785
		2.0		-3.19087	-3.11214	-3.61977	-3.53466
		3.0		-2.54915	-2.56668	-2.87576	-2.90889
			1.0	-2.54915	-2.56668	-2.87576	-2.90889
			2.0	-5.98723	-5.78705	-6.84322	-6.61448
			3.0	-7.15771	-7.19576	-8.15955	-8.23057

5. Conclusions

This study investigate the case of three dimensional micropolar nanofluids of single and multi-walled carbon nanotubes (CNTs) dissolved in water and gasoline liquids for the first time reported to the case of so-called B*ö*dewadt flow, which occurs when a fluid rotates at a

sufficiently great distance from a stationary disk. The stationary disk is then stretched linearly in the radial direction. Darcy-Forchheimer porous media is also considered. Heat transport in the appearance of radiation and viscous dissipation is examined. The nonlinear equation describing the flow problem is converted to nonlinear ODEs using similarity transformation, which is then solved using shooting method (bvp4c technique).

The study's finding led to the following conclusions:

- It is shown that as the value of ϕ, λ, and K increased, so did the axial velocity $h(\eta)$, whereas the value of R increased, the axial velocity $h(\eta)$ declined.
- The radial velocity $f(\eta)$ and tangential velocity $g(\eta)$ are decreases as ϕ, λ, and K increases, whereas they are increases as R increase.
- Micro-rotational redial velocity $L(\eta)$ upsurges for rising value of ϕ and decay down for growing values of R, λ, K, α_1, and α_2.
- Micro-rotational tangential velocity $M(\eta)$ upturns with raise in ϕ, λ, α_1, and α_2, however the velocity decline with growth in R and K.
- The temperature distribution decline for large value of ϕ and λ, while, temperature is upturns when R and K grow up.
- Skin friction decay down when ϕ and λ rise up, while skin friction upsurges for rising values of R and K.
- Nusselt number rise up for rising values of ϕ and λ, while fall down for growing values of R and K.

- It was also discovered that the effect of multiple-walled CNTs is quite effective than that of single-walled CNTs. When compared to water-based fluids, gasoline oil also displays an overarching trend.

Funding: "The project was financed by Project financed by Lucian Blaga University of Sibiu through research grant LBUS-IRG-2022-08".

References

[1] S. U. S. Choi and J. A. Eastman, "Enhancing thermal conductivity of fluids with nanoparticles," *ASME Int. Mech. Eng. Congr. Expo.*, no. 10, pp. 12a – 17, 1995.

[2] M. M. Elias *et al.*, "Effect of nanoparticle shape on the heat transfer and thermodynamic performance of a shell and tube heat exchanger," *Int. Commun. Heat Mass Transf.*, vol. 44, pp. 93–99, May 2013, doi: 10.1016/J.ICHEATMASSTRANSFER.2013.03.014.

[3] M. M. Elias, I. M. Shahrul, I. M. Mahbubul, R. Saidur, and N. A. Rahim, "Effect of different nanoparticle shapes on shell and tube heat exchanger using different baffle angles and operated with nanofluid," *Int. J. Heat Mass Transf.*, vol. 70, pp. 289–297, 2014, doi: 10.1016/J.IJHEATMASSTRANSFER.2013.11.018.

[4] M. Sheikholeslami and M. M. Bhatti, "INFLUENCE OF EXTERNAL MAGNETIC SOURCE ON NANOFLUID TREATMENT IN A POROUS CAVITY," *J. Porous Media*, vol. 22, no. 12, pp. 1475–1491, 2019, doi: 10.1615/JPORMEDIA.2019024518.

[5] H. Hajabdollahi and Z. Hajabdollahi, "Investigating the effect of nanoparticle on thermo-economic optimization of fin and tube heat exchanger," *Proc. Inst. Mech. Eng. Part E J. Process Mech. Eng.*, vol. 231, no. 6, pp. 1127–1140, Dec. 2017, doi: 10.1177/0954408916656677.

[6] N. A. Shah, A. Wakif, E. R. El-Zahar, T. Thumma, and S. J. Yook, "Heat transfers thermodynamic activity of a second-grade ternary nanofluid flow over a vertical plate with Atangana-Baleanu time-fractional integral," *Alexandria Eng. J.*, vol. 61, no. 12, pp. 10045–10053, Dec. 2022, doi: 10.1016/J.AEJ.2022.03.048.

[7] A. Dawar, A. Wakif, A. Saeed, Z. Shah, T. Muhammad, and P. Kumam, "Significance of Lorentz forces on Jeffrey nanofluid flows over a convectively heated flat surface featured by multiple velocity slips and dual stretching constraint: a homotopy analysis approach," *J. Comput. Des. Eng.*, vol. 9, no. 2, pp. 564–582, Apr. 2022, doi: 10.1093/JCDE/QWAC019.

[8] R. J. P. Gowda, A. Rauf, R. Naveen Kumar, B. C. Prasannakumara, and S. A. Shehzad, "Slip flow of Casson–Maxwell nanofluid confined through stretchable disks," *Indian J. Phys.*, vol. 96, no. 7, pp. 2041–2049, Jun. 2022, doi: 10.1007/S12648-021-02153-7/FIGURES/17.

[9] R. Naveen Kumar, S. Suresha, R. J. P. Gowda, S. B. Megalamani, and B. C. Prasannakumara, "Exploring the impact of magnetic dipole on the radiative nanofluid flow over a stretching sheet by means of KKL model," *Pramana 2021 954*, vol. 95, no. 4, pp. 1–9, Oct. 2021, doi: 10.1007/S12043-021-02212-Y.

[10] S. Hosseinzadeh, K. Hosseinzadeh, A. Hasibi, and D. D. Ganji, “Thermal analysis of moving porous fin wetted by hybrid nanofluid with trapezoidal, concave parabolic and convex cross sections,” *Case Stud. Therm. Eng.*, vol. 30, p. 101757, Feb. 2022, doi: 10.1016/J.CSITE.2022.101757.

[11] S. Hosseinzadeh, K. Hosseinzadeh, A. Hasibi, and D. D. Ganji, “Hydrothermal analysis on non-Newtonian nanofluid flow of blood through porous vessels:,” *https://doi.org/10.1177/09544089211069211*, Jan. 2022, doi: 10.1177/09544089211069211.

[12] K. Hosseinzadeh *et al.*, “Entropy generation of three-dimensional Bödewadt flow of water and hexanol base fluid suspended by Fe₃O₄ and MoS₂ hybrid nanoparticles,” *Prama*, vol. 95, no. 2, p. 57, Jun. 2021, doi: 10.1007/S12043-020-02075-9.

[13] Y. M. Chu, S. Bashir, M. Ramzan, and M. Y. Malik, “Model-based comparative study of magnetohydrodynamics unsteady hybrid nanofluid flow between two infinite parallel plates with particle shape effects,” *Math. Methods Appl. Sci.*, 2022, doi: 10.1002/MMA.8234.

[14] W. F. Xia, I. L. Animasaun, A. Wakif, N. A. Shah, and S. J. Yook, “Gear-generalized differential quadrature analysis of oscillatory convective Taylor-Couette flows of second-grade fluids subject to Lorentz and Darcy-Forchheimer quadratic drag forces,” *Int. Commun. Heat Mass Transf.*, vol. 126, p. 105395, Jul. 2021, doi: 10.1016/J.ICHEATMASSTRANSFER.2021.105395.

[15] M. I. Afridi, A. Wakif, A. K. Alanazi, Z. M. Chen, M. U. Ashraf, and M. Qasim, “A comprehensive entropic scrutiny of dissipative flows over a thin needle featured by variable thermophysical properties,” *https://doi.org/10.1080/17455030.2022.2049922*, 2022, doi: 10.1080/17455030.2022.2049922.

[16] W. Jamshed, K. S. Nisar, R. J. P. Gowda, R. N. Kumar, and B. C. Prasannakumara, “Radiative heat transfer of second grade nanofluid flow past a porous flat surface: a single-phase mathematical model,” *Phys. Scr.*, vol. 96, no. 6, p. 064006, Apr. 2021, doi: 10.1088/1402-4896/ABF57D.

[17] R. J. Punith Gowda *et al.*, “Thermophoretic particle deposition in time-dependent flow of hybrid nanofluid over rotating and vertically upward/ downward moving disk,” *Surfaces and Interfaces*, vol. 22, p. 100864, Feb. 2021, doi: 10.1016/J.SURFIN.2020.100864.

[18] A. Hamid, Y. M. Chu, M. I. Khan, R. N. Kumar, R. J. P. Gowd, and B. C. Prasannakumara, “Critical values in axisymmetric flow of magneto-Cross nanomaterial towards a radially shrinking disk,” *https://doi.org/10.1142/S0217979221501058*, vol. 35, no. 7, Apr. 2021, doi: 10.1142/S0217979221501058.

[19] K. Hosseinzadeh, S. Salehi, M. R. Mardani, F. Y. Mahmoudi, M. Waqas, and D. D. Ganji, “Investigation of nano-Bioconvective fluid motile microorganism and nanoparticle flow by considering MHD and thermal radiation,” *Informatics Med. Unlocked*, vol. 21, p. 100462, Jan. 2020, doi: 10.1016/J.IMU.2020.100462.

[20] K. Hosseinzadeh, A. Asadi, A. R. Mogharrebi, M. Ermia Azari, and D. D. Ganji, “Investigation of mixture fluid suspended by hybrid nanoparticles over vertical cylinder by considering shape factor effect,” *J. Therm. Anal. Calorim. 2020 1432*, vol. 143, no. 2, pp. 1081–1095, Jan. 2020, doi: 10.1007/S10973-020-09347-X.

[21] K. U. Rehman, W. Shatanawi, and M. Y. Malik, “Heat transfer and double sampling of stratification phenomena in non-Newtonian liquid suspension: A comparative thermal analysis,”

Case Stud. Therm. Eng., vol. 33, p. 101934, May 2022, doi: 10.1016/J.CSITE.2022.101934.

[22] A. Salmi, H. A. Madkhali, M. Nawaz, S. O. Alharbi, and M. Y. Malik, "Computational analysis for enhancement of heat and mass transfer in MHD-polymer with hybrid nano-particles using generalized laws," *Case Stud. Therm. Eng.*, vol. 31, p. 101851, Mar. 2022, doi: 10.1016/J.CSITE.2022.101851.

[23] T. Hayat, Z. Hussain, A. Alsaedi, and B. Ahmad, "Heterogeneous-homogeneous reactions and melting heat transfer effects in flow with carbon nanotubes," *J. Mol. Liq.*, vol. 220, pp. 200–207, Aug. 2016, doi: 10.1016/J.MOLLIQ.2016.04.012.

[24] A. Hussanan, I. Khan, M. R. Gorji, and W. A. Khan, "CNTS-Water–Based Nanofluid Over a Stretching Sheet," *Bionanoscience*, vol. 9, no. 1, pp. 21–29, Mar. 2019, doi: 10.1007/S12668-018-0592-6.

[25] T. Hayat, F. Haider, T. Muhammad, and A. Alsaedi, "Numerical treatment for Darcy-Forchheimer flow of carbon nanotubes due to an exponentially stretching curved surface," *J. Cent. South Univ.*, vol. 26, no. 4, pp. 865–872, Apr. 2019, doi: 10.1007/S11771-019-4055-1.

[26] T. Muhammad, D. C. Lu, B. Mahanthesh, M. R. Eid, M. Ramzan, and A. Dar, "Significance of Darcy-Forchheimer Porous Medium in Nanofluid Through Carbon Nanotubes," *Commun. Theor. Phys.*, vol. 70, no. 3, pp. 361–366, Sep. 2018, doi: 10.1088/0253-6102/70/3/361.

[27] K. Muhammad, T. Hayat, A. Alsaedi, and S. Asghar, "Stagnation point flow of basefluid (gasoline oil), nanomaterial (CNTs) and hybrid nanomaterial (CNTs + CuO): A comparative study," *Mater. Res. Express*, vol. 6, no. 10, Aug. 2019, doi: 10.1088/2053-1591/AB356E.

[28] L. J. Crane, "Flow past a stretching plate," *Zeitschrift für Angew. Math. und Phys. ZAMP*, vol. 21, no. 4, pp. 645–647, Jul. 1970, doi: 10.1007/BF01587695.

[29] M. M. Rashidi, N. Vishnu Ganesh, A. K. Abdul Hakeem, and B. Ganga, "Buoyancy effect on MHD flow of nanofluid over a stretching sheet in the presence of thermal radiation," *J. Mol. Liq.*, vol. 198, pp. 234–238, 2014, doi: 10.1016/J.MOLLIQ.2014.06.037.

[30] M. Turkyilmazoglu, "Bödewadt flow and heat transfer over a stretching stationary disk," *Int. J. Mech. Sci.*, vol. 90, pp. 246–250, Jan. 2015, doi: 10.1016/J.IJMECSCI.2014.10.022.

[31] M. Mustafa, J. A. Khan, T. Hayat, and A. Alsaedi, "On Bödewadt flow and heat transfer of nanofluids over a stretching stationary disk," *J. Mol. Liq.*, vol. 211, pp. 119–125, Nov. 2015, doi: 10.1016/J.MOLLIQ.2015.06.065.

[32] M. Gnaneswara Reddy, R. J. Punith Gowda, R. Naveen Kumar, B. C. Prasannakumara, and K. Ganesh Kumar, "Analysis of modified Fourier law and melting heat transfer in a flow involving carbon nanotubes:," *https://doi.org/10.1177/09544089211001353*, vol. 235, no. 5, pp. 1259–1268, Mar. 2021, doi: 10.1177/09544089211001353.

[33] M. Gholinia, K. Hosseinzadeh, and D. D. Ganji, "Investigation of different base fluids suspend by CNTs hybrid nanoparticle over a vertical circular cylinder with sinusoidal radius," *Case Stud. Therm. Eng.*, vol. 21, p. 100666, Oct. 2020, doi: 10.1016/J.CSITE.2020.100666.

[34] M. K. Nayak, A. Wakif, I. L. Animasaun, and M. S. H. Alaoui, "Numerical Differential Quadrature Examination of Steady Mixed Convection Nanofluid Flows Over an Isothermal Thin Needle Conveying Metallic and Metallic Oxide Nanomaterials: A Comparative Investigation,"

Arab. J. Sci. Eng. 2020 457, vol. 45, no. 7, pp. 5331–5346, Feb. 2020, doi: 10.1007/S13369-020-04420-X.

[35] A. Wakif, I. L. Animasaun, U. Khan, N. A. Shah, and T. Thumma, "Dynamics of radiative-reactive Walters-b fluid due to mixed convection conveying gyrotactic microorganisms, tiny particles experience haphazard motion, thermo-migration, and Lorentz force," *Phys. Scr.*, vol. 96, no. 12, p. 125239, Oct. 2021, doi: 10.1088/1402-4896/AC2B4B.

[36] A. Eringen, "THEORY OF MICROPOLAR FLUIDS," *undefined*, vol. 16, no. 1, pp. 1–18, 1966, doi: 10.1512/IUMJ.1967.16.16001.

[37] R. Bhargava, L. Kumar, and H. S. Takhar, "Numerical solution of free convection MHD micropolar fluid flow between two parallel porous vertical plates," *Int. J. Eng. Sci.*, vol. 41, no. 2, pp. 123–136, Jan. 2003, doi: 10.1016/S0020-7225(02)00157-X.

[38] R. Ul Haq, S. Nadeem, N. S. Akbar, and Z. H. Khan, "Buoyancy and radiation effect on stagnation point flow of micropolar nanofluid along a vertically convective stretching surface," *IEEE Trans. Nanotechnol.*, vol. 14, no. 1, pp. 42–50, Jan. 2015, doi: 10.1109/TNANO.2014.2363684.

[39] S. Nadeem and N. Abbas, "On both MHD and slip effect in micropolar hybrid nanofluid past a circular cylinder under stagnation point region," *Can. J. Phys.*, vol. 97, no. 4, pp. 392–399, 2019, doi: 10.1139/CJP-2018-0173/ASSET/IMAGES/CJP-2018-0173IEQ3.GIF.

[40] N. Abbas, S. Saleem, S. Nadeem, A. A. Alderremy, and A. U. Khan, "On stagnation point flow of a micro polar nanofluid past a circular cylinder with velocity and thermal slip," *Results Phys.*, vol. 9, pp. 1224–1232, Jun. 2018, doi: 10.1016/J.RINP.2018.04.017.

[41] F. E. Alsaadi, K. Muhammad, T. Hayat, A. Alsaedi, and S. Asghar, "Numerical study of melting effect with entropy generation minimization in flow of carbon nanotubes," *J. Therm. Anal. Calorim. 2019 1401*, vol. 140, no. 1, pp. 321–329, Sep. 2019, doi: 10.1007/S10973-019-08720-9.

[42] Q. Z. Xue, "Model for thermal conductivity of carbon nanotube-based composites," *Phys. B Condens. Matter*, vol. 368, no. 1–4, pp. 302–307, Nov. 2005, doi: 10.1016/J.PHYSB.2005.07.024.

[43] N. A. Khan, S. Khan, and A. Ara, "Flow of micropolar fluid over an off centered rotating disk with modified Darcy's law," *Propuls. Power Res.*, vol. 6, no. 4, pp. 285–295, Dec. 2017, doi: 10.1016/J.JPPR.2017.11.006.

[44] M. Alghamdi, A. Wakif, T. Thumma, U. Khan, D. Baleanu, and G. Rasool, "Significance of variability in magnetic field strength and heat source on the radiative-convective motion of sodium alginate-based nanofluid within a Darcy-Brinkman porous structure bounded vertically by an irregular slender surface," *Case Stud. Therm. Eng.*, vol. 28, p. 101428, Dec. 2021, doi: 10.1016/J.CSITE.2021.101428.

[45] L. A. Lund, A. Wakif, Z. Omar, I. Khan, and I. L. Animasaun, "Dynamics of water conveying copper and alumina nanomaterials when viscous dissipation and thermal radiation are significant: Single-phase model with multiple solutions," *Math. Methods Appl. Sci.*, Apr. 2022, doi: 10.1002/MMA.8270.

[46] A. Wakif, M. Zaydan, A. S. Alshomrani, T. Muhammad, and R. Sehaqui, "New insights into the dynamics of alumina-(60% ethylene glycol + 40% water) over an isothermal stretching sheet using a renovated Buongiorno's approach: A numerical GDQLLM analysis," *Int. Commun. Heat Mass Transf.*, vol. 133, p. 105937, Apr. 2022, doi: 10.1016/J.ICHEATMASSTRANSFER.2022.105937.

[47] L. A. Lund, A. Wakif, Z. Omar, I. Khan, and I. L. Animasaun, "Dynamics of water conveying copper and alumina nanomaterials when viscous dissipation and thermal radiation are significant: Single-phase model with multiple solutions," *Math. Methods Appl. Sci.*, 2022, doi: 10.1002/MMA.8270.

[48] K. Hosseinzadeh, S. Roghani, A. R. Mogharrebi, A. Asadi, M. Waqas, and D. D. Ganji, "Investigation of cross-fluid flow containing motile gyrotactic microorganisms and nanoparticles over a three-dimensional cylinder," *Alexandria Eng. J.*, vol. 59, no. 5, pp. 3297–3307, Oct. 2020, doi: 10.1016/J.AEJ.2020.04.037.

[49] K. Hosseinzadeh, M. R. Mardani, S. Salehi, M. Paikar, and D. D. Ganji, "Investigation of Micropolar Hybrid Nanofluid (Iron Oxide–Molybdenum Disulfide) Flow Across a Sinusoidal Cylinder in Presence of Magnetic Field," *Int. J. Appl. Comput. Math.*, vol. 7, no. 5, Oct. 2021, doi: 10.1007/S40819-021-01148-6.

[50] S. Hosseinzadeh, K. Hosseinzadeh, M. Rahai, and D. D. Ganji, "Analytical solution of nonlinear differential equations two oscillators mechanism using Akbari–Ganji method," *https://doi.org/10.1142/S0217984921504625*, vol. 35, no. 31, Aug. 2021, doi: 10.1142/S0217984921504625.

[51] M. Fakour, D. D. Ganji, and M. Abbasi, "Scrutiny of underdeveloped nanofluid MHD flow and heat conduction in a channel with porous walls," *Case Stud. Therm. Eng.*, vol. 4, pp. 202–214, Nov. 2014, doi: 10.1016/J.CSITE.2014.10.003.

- ***Micropolar nanofluids of SWCNTS and MWCNTS dissolved in water and gasoline liquids is modeled***
- ***Bödewadt fluid flow with heat transport in the appearance of radiation and convection is examined.***
- ***Fluid rotates at an adequate great distance out of a static disk is stretched linearly in the radial direction.***
- ***The Darcy-Forchheimer porous media is also taken into account.***
- ***The finding indicates that the volume fraction enhanced, the micro-rotational velocities enhances.***

Competing Interests statement: The author declares that they have no competing interests